Computer Algorithm for Simulation of the Human Optical System and Contribution of the Cornea to the Optical Imperfections of the Eye

Luis Alberto Carvalho*

Instituto de Física de São Carlos-Grupo de Óptica

Av. Dr. Carlos Botelho, 1465, 13560-970, São Carlos – SP

and *UNIFESP - Universidade Federal de São Paulo, Escola Paulista de Medicina*

lavc@if.sc.usp.br, luis@adage.berkeley.edu

The main objective of this work is to demonstrate the relation between corneal surface imperfections and retinal image imperfections. Its originality resides on the fact that specialized literature approximate the eye and the cornea as mathematical surfaces to explain simple refraction problems (myopic, hyperopic, astigmatic), whereas in the present work we have used topographic data for *in vivo* corneas and other refractive imperfections may be analyzed. This data was collected in a specialized instrument denominated *Corneal Topographer*. With this true corneal data we could understand how more complex imperfections, directly related to more delicate surface curvature differences, degrade the retinal images. It is well known that the cornea contributes to approximately 2/3 of the total refraction of the eye. Nevertheless, there is very few knowledge of its contribution to the optical aberrations of the images formed at the retina. Most corneal diagnostic equipments (Corneal Topographers and Keratometers) measure only its dioptric power (proportional to curvature) and, in certain cases, shape, but do not calculate or estimate the corneal contribution to the quality of image formation at the retina. On the other hand, auto-refractors and wave-front sensors measure the optical aberrations of the eye as a single optical "device", and therefore do not indicate individual contributions. We have developed algorithms that read elevation data from a commercial corneal topographer and use this data and ray-tracing algorithms to estimate the image quality formed at the retina. Conventional optical design test functions such as the Point Spread Function (PSF) and longitudinal shift in focus position, together with the two-dimensional curvature maps obtained from corneal topography, are plotted and used to analyze retinal image quality.

O objetivo principal deste trabalho é mostrar a relação entre as imperfeições da córnea e as imperfeições das imagens formadas na retina. Trata-se de um tema original visto que na literatura especializada são usados apenas modelos matemáticos aproximados do olho e da córnea para explicar problemas simples de refração (astigmatismo, miopia e hipermetropia), sendo que no atual trabalho utilizamos dados de córneas *in vivo*. Estes dados foram colhidos num instrumento especializado denominado *Topógrafo de Córnea*. Com isso pudemos entender como imperfeições mais complexas, relacionadas diretamente a diferenças sutis na curvatura da superfície da córnea, degradam a imagem da retina. Sabe-se que a córnea é responsável por aproximadamente 2/3 da refração total do olho. No entanto, há pouca informação a respeito da influência das aberrações ópticas da córnea na formação das imagens na retina. A maioria dos equipamentos de diagnóstico da superfície da córnea (ceratômetro, topógrafo de córnea) mede apenas o poder óptico da mesma (proporcional à curvatura) e, em alguns casos, a forma tri-dimensional. No entanto, não há estimativa das contribuições da córnea na formação de imagens no fundo do olho. Por outro lado, auto-refratores e modernos instrumentos chamados "Wave-Front" medem toda refração do olho como se este fosse um sistema óptico constituído por uma única lente, e, portanto não considera individualmente as contribuições do cristalino e da córnea. Neste trabalho foram desenvolvidos algoritmos que lêem dados topográficos de córneas *in vivo* mensuradas em um aparelho comercial, depois fazem um traçado de raios para estimar a imagem formada na retina de um olho padrão. Funções convencionais para testes ópticos, como a "Point Spread Function" (PSF) e deslocamento longitudinal na posição do foco (aberração longitudinal), juntamente com mapas bidimensionais de curvatura da córnea (em Dioptrias), obtidos dos dados da topografia de córnea, são impressos e utilizados para analisar a qualidade das imagens da retina.

---

1   Introduction

The interest for the physiological and optical properties of the human eye, and how they are related in terms of visual quality, come from very ancient times [1]. A very thorough study was undertaken by Helmholtz in the 19th century and was compiled by himself in the famous collection *Helmholtz Treatese in Phisiological Optics* [2]. From this time up to modern days an incredible amount of techniques and instrumentation for visual quality measurements were implemented. Today they form a collection of tools that aid the eye- care professional in providing the best diagnostic and treatment available to their patients.

With the advent of refractive surgeries for correction of myopia in the early 80's, better instrumentation was required in order to analyze the pre and post shape of the entire corneal surface. The earlier techniques such as manual keratometers [3, 4], which measure only the central 3 mm, were no longer sufficient. With the advent of more powerful low cost microcomputers a new line of equipments for corneal surface analysis started to take place of the conventional keratometers. These instruments, popularly known as *Corneal Topographers*, are based on the 19th century Placido Disc [5], but surface curvature and calculations are based on sophisticated image processing [6, 7] and computer graphics techniques for surface reconstruction [8, 9]. They allow the eye-care professional to analyze a 8-10 mm in diameter region over the cornea, displaying curvature data for thousands of points.

The first refractive surgery techniques (*RK – Radial Keratectomy*) were based on the application of radial incisions to flatten the central cornea. This was an empiric method and based on data collected from human cadavers and animal eyes. During this same period certain companies and research laboratories started to investigate an alternative method for corneal intervention. At the end of the 1980's and beginning of the 1990's some companies made available for tests the first ex<u>ci</u>ted <u>dim</u>mer laser for corneal tissue ablations. These lasers became popularly known as *excimer* lasers and the first generations were primarily designed for myopic correction, and procedures became commonly known as *PRK – <u>P</u>hoto<u>r</u>efractive <u>K</u>eratectomy*. These lasers rapidly took over the place of conventional RK techniques, which were very aggressive to the corneal tissue since incisions could go as deep as 90% of the corneal depth. In the late 1990s and beginning of this century a series of technological advances allowed refractive surgery to be taken to higher levels of precision and there fore patient satisfaction. Excimer lasers with flying spot beams and eye tracking systems (to eliminate misalignment of laser treatment caused by involuntary eye movements) provide sufficient precision for practically sculpting the cornea to any desired shape [10, 11] and a high resolution auto-refractor inspired in astronomical instruments [12] measures the eye's wave-front optical aberrations with such a high precision, that refractive surgery can now be undertaken in a patient-to-patient base, allowing what became known as *customized corneal abla-*

tions.

With the advent of these techniques other important questions arrived. For instance: what is the best correction for the aberrations of an eye? Does the lens accommodation process influence on this choice? If it does, than should one determine the best ablation profile based on age factors, such as presbyopia?

These and other questions still have no answer and in this work we are attempting to solve the relation between corneal imperfections and retinal image imperfections. This is only part of the problem. Further research should attempt to answer questions related directly to the crystalline lens, such as presbyopia mentioned above. The originality of our present work resides on the fact that we are not using a purely theoretical eye to understand low order aberrations (myopic, hyperopic, astigmatic). These are already very well understood. Instead, we are using a simple model eye with no crystalline, and instead of a mathematical model surface for the cornea (such as a sphere or a ellipsoid) we are attaching topographical data from *in vivo* corneas measured in a sophisticated device called *Videokeratograph* (or *Corneal Topographer*). This allows us to understand how corneal imperfections degrade images formed at the fovea.

Algorithms based on a hybrid mathematical/biological model eye and computer graphics visualization and raytracing techniques [13]. As we'll see, our preliminary eye model, different from those in literature, has *in vivo* corneal topography data for voluntary individuals applied to a schematic eye globe, based on statistical data. In a previous joint work with the Computer Science Department of the Universidade de São Paulo (ICMC) [14] a simulation of Snellen optotypes was implemented also using true corneal topography from our Corneal Topography equipment [15, 16]. The difference is that in the previous work a sophisticated ray tracing software package was used (VTK – Visualization Toolkit [17, 18]) and the visualization approach of the retinal images were different from the one presented in this article. Also, in this work we have worked out the ray tracing equations one by one and used a different modeling tool (Matlab, www.mathworks.com) to implement the algorithms and visualization. We believe this technique can lead to further contributions to the understanding and visualization of the optical imperfections of the eye and planning process for customized refractive surgeries.

2   Material and Methods

Eye model

There are several schematic models for the human eye, from very traditional models [2, 3, 4] to modern ones [19]. One of the most popular is that of Gullstrand which is a simplification of Helmholtz's eye model [2]. Although this model is reasonably accurate, there are several other models in the literature that have, each one, its own advantages depending on the desired application. In our specific case we do not dispose of lens data of each patient so we decided not

to use statistical data for the accommodated lens. Instead we use a model eye, known as Emsley Schematic Eye, that substitutes the lens and cornea for a single refractive surface and an equivalent refractive index for the interior of the eye (see Figure 1), such that the lens power is taken into account

in this index so there is no need to apply it's shape and specific indexes. The main advantage of this eye is that we may simply "attach" to it our corneal topography data and apply the ray tracing all the way to the retina.
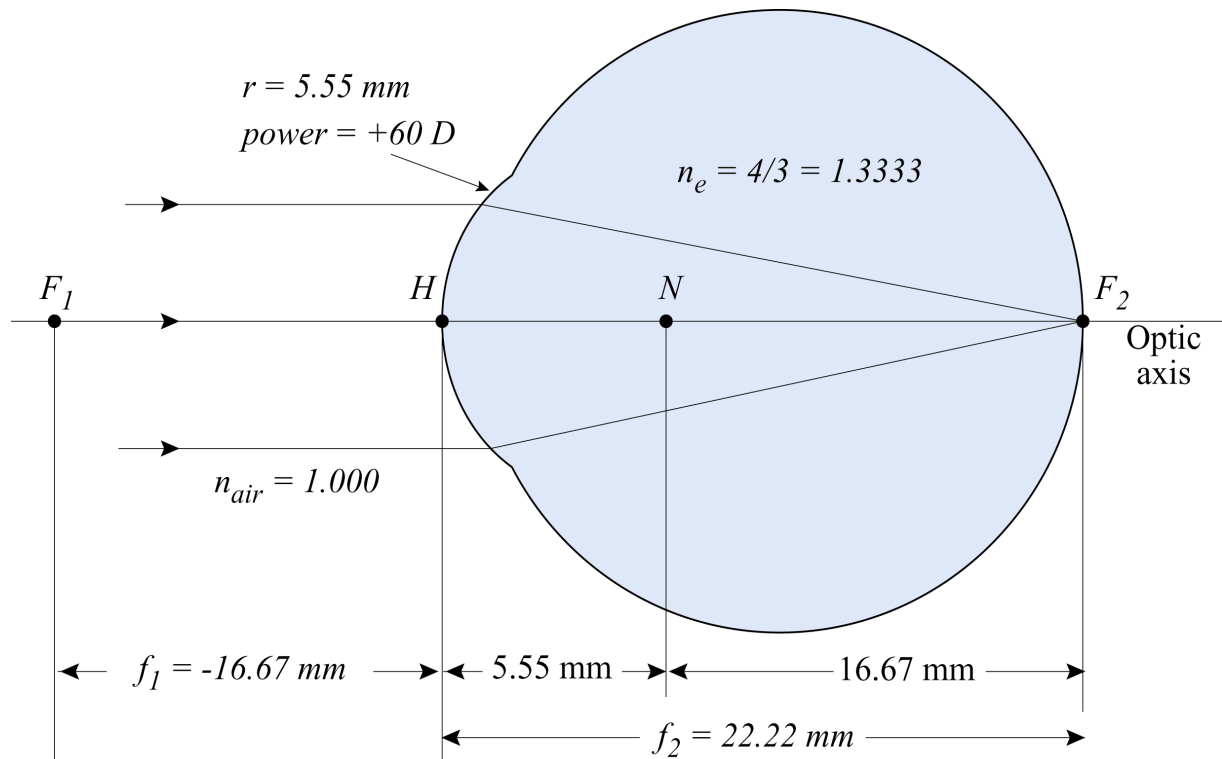

Figure 1. Emsley squematic eye and parameters.

The axial distance for this eye is 22.22 mm. The net dioptric power of the eye is due to the single corneal surface and has value of 60D for a 5.55 mm radius cornea shown in the diagram. This is the refracting surface that we'll be replacing with our topography data for *in vivo* eyes. The refractive index of the entire eye is 1.333.

The corneal topography data was collected from an instrument developed previously in our own laboratory at the IFSC – USP [15, 16], for which the main principle is shown in Figure 2. This instrument consists of a conic pattern with concentric black and white discs (usually referred to as Placido Discs, after its inventor [5]) painted on its surface that faces the cornea and on its back illuminated by "donut" shaped fluorescent lamp. The image reflected from the cornea is amplified by an optical system and focused at a CCD camera also behind the Placido Disc. The CCD signal is sent to a frame grabber installed on a Pentium III 600 MHz microcomputer, running *Microsoft Windows 98* OS. The programming languages used for software implementation are *Borland's Delphi 4.0-6.0 and Paradox 7.0.* The digitized Placido images are processed using conventional image processing techniques [6] and the extracted informa-

tion is then inserted in mathematical algorithms for retrieval of corneal shape and curvature [16, 20]. This data is manipulated in the desired way since we have access to all the original code, which was implemented previously. For this specific project we chose to save the corneal data in ASCII files containing three types of information in cylindrical coordinates (please see Figure 3 for coordinate system scheme): the corneal dioptric power, proportional to curvature (*diop.txt*), corneal height or elevation in the positive z direction (*z_c.txt*), and Placido image disc edge positions in the radial direction ρ (*rho_c.txt*).

Ray-tracing Scheme

The coordinate system chosen and ray-tracing scheme may be seen in Figure 3.

Since we have corneal topography data for 360 semi-meridians (angle θ) we consider data for each semi-meridian one at a time. This means that our ray-tracing procedure happens in a two-dimensional plane, which is a slice of the cornea containing the optic axis z and the semi-meridian at angle θ. An initial ray of light with direction defined by the unit vector $\hat{V}_i$ hits the cornea at point (ρ_c, θ_c). Since we

consider light coming from an object point located at infinity (>6m) the unit vector is

$$\hat{V}_i = \hat{k} \tag{1}$$

and therefore is parallel to the z axis. Notice that this is not a paraxial approximation since the incident rays will hit the cornea a several points close and far from the z axis. This is actually a very important fact since one of our objectives is to find out what happens with the image quality at the retina for peripheral rays. In order to calculate the direction of the refracted ray we need to now the normal vector to the surface at point (ρ_c, θ_c), which may be written as
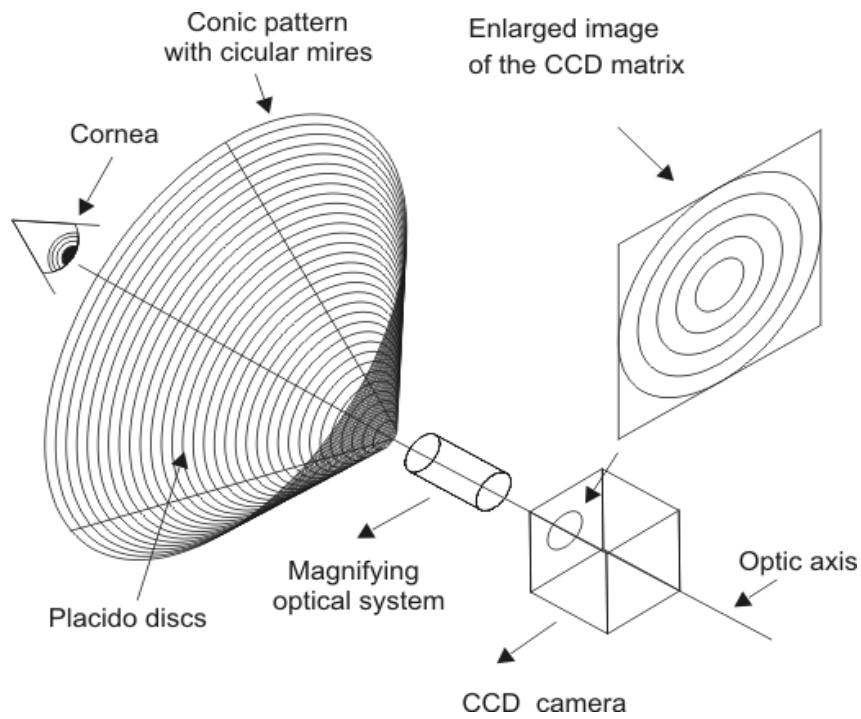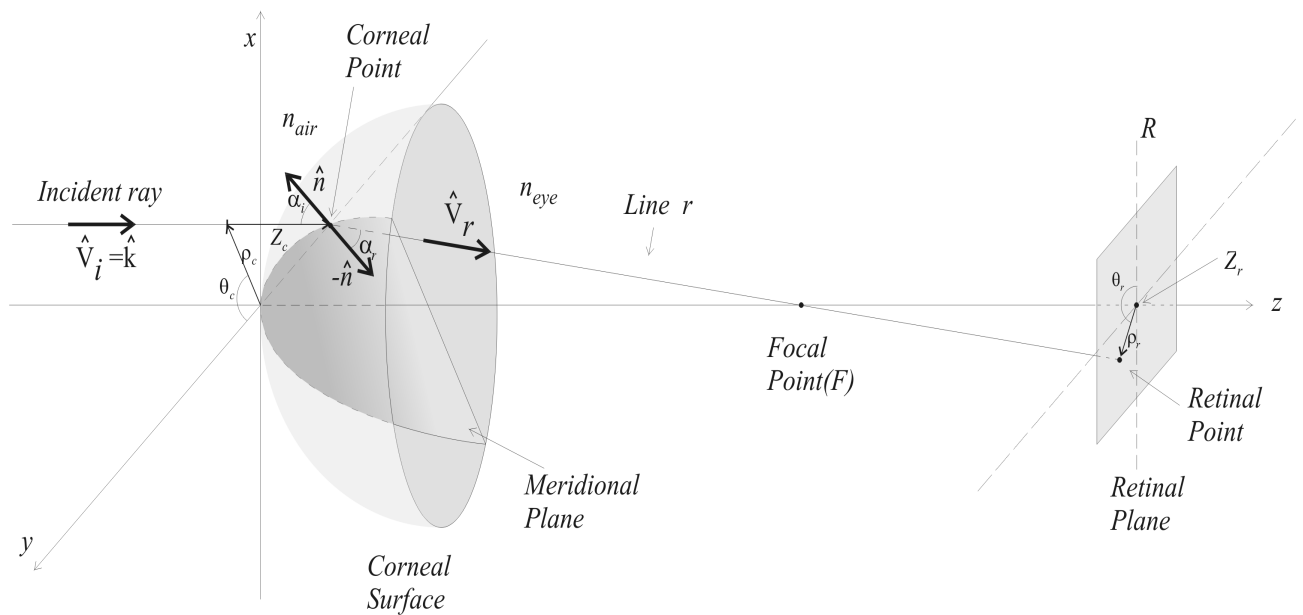
Figure 2. Optical principle of the corneal topographer.

Figure 3. Ray tracing scheme.

$$\hat{n} = \cos\alpha_i(-\hat{k}) + sen\alpha_i\hat{\rho} \tag{2}$$

where $\hat{\rho}$ is the unit vector in the radial direction and angle α_i is the incident angle formed between the incident vector $\hat{V}_i$ and the corneal normal $\hat{n}$. From the slice shown in Figure 3, α_i may be written as

$$\alpha_i = arcsen(\rho/R) \tag{3}$$

where R is the axial radius of curvature of the cornea at point (ρ_c, θ_c). It is calculated from the dioptric power (D) file (*diop.txt*) and equation

$$D = \frac{(n_c - 1)}{R} \tag{4}$$

where D is the dioptric power (or axial curvature, as some like to refer to [21]) used in ophthalmic instruments, R is the radius of curvature in meters and n_c is the equivalent refracted index of the cornea and internal optics of the Emsley eye (given in Table 1). From the angle of incidence and the incident vector we may calculate the refracted vector using Snell's Law in its vector form

$$n_c\hat{V}_i = n_{air}\hat{V}_r + \gamma\hat{n} \tag{5}$$

where n_{air} is the refraction index of air (for which we use the value 1) and

$$\gamma = n_c\cos\alpha_r - n_{air}\cos\alpha_i \tag{6}$$

from equations (5) and (6) we may calculate the refracting vector components

$$\hat{V}_r = \begin{pmatrix} V_{r\rho} \\ V_{rz} \end{pmatrix} \tag{7}$$

and therefore the parametric equation of line r:

$$\begin{pmatrix} \rho \\ z \end{pmatrix} = \begin{pmatrix} \rho_c \\ z_c \end{pmatrix} + t\begin{pmatrix} V_{r\rho} \\ V_{rz} \end{pmatrix} \tag{8}$$

Now that we have the parametric equation of the refracted ray we may calculated the two parameters of interest, i. e., the focal distance (z_f) along the z axis and the point of intersection with the retinal plane (ρ_r, θ_r). In order to do this we find the parameter t when $\rho = 0$. From (8) we have

$$t_f = \frac{\rho_c}{V_{i\rho}} \tag{9}$$

and then substitute this value in

$$z_f = z_c + V_{iz}t_f \tag{10}$$

and the retinal point parameter is

$$t_r = \frac{z_r - z_c}{V_{iz}} \tag{11}$$

and the retinal point coordinates are then given by applying the value t_r in equation and (8).

Using equations (5) – (11) 16 rays were traced for each of 360 semi-meridians (θ) separated by 1^0 angles, totalizing 5760 rays for each cornea. We also applied techniques commonly used in optical design softwares (see CODE V at www.opticalres.com, or ZEEMAX at http://www.focus-software.com, for example) to visualize the quality of the images at the retinal plane (PSF – Point Spread Function) and color maps of the corneal topography (axial curvature) for comparison. We following present results for the 4 corneas analyzed.

3   Results

4 corneas of the right eyes of 4 healthy voluntaries were examined at the corneal topographer. The keratometry of each cornea may be seen in Table 1 and the axial curvature map of each cornea may be seen in Figure 4. Although many other corneas could be examined, corneas were chosen such that they represented specific but common pathologies: the first cornea (A) is considered a "normal" cornea since it has regular curvature along all meridians and represent the desired type of cornea for a healthy eye; the second (B) and fourth (D) corneas are with-the-rule astigmatisms, but we chose a severe astigmatic and a moderate astigmatic in order to evaluate their differences; the third cornea (C), keratoconic, is more rare in the population, but since it represents one of the corneal pathologies that most degrade visual acuity, we decided to analyze an example of a severe case here.

Data files (*z_c.txt, rho_c.txt and diop.txt*) for each exam were inserted in a *Matlab* (see www.mathworks.com) codification of the algorithm described in equations (5) – (11). Figures 5-8 show results for each case.

Notice in Figure 6 from the SL graph that the focusing distance decreases as the pupil dilates, but contrary to the "normal" cornea (A), curves are totally different for the vertical and horizontal semi-meridians, which is expected since this eye has greater with the rule astigmatism. The SR is also in accordance to the expected variation in retinal image size for the four semi-meridians, but this time the four curves are not so close to each other, as it should be for an astigmatic cornea. The PSF in the IL graph shows symmetric rings but in elliptic form, i. e., closer to each other in the vertical meridian and, as expected, the IR graph shows a small variation in axial curvature from center to periphery of the cornea, with vertical and horizontal meridians varying differently.

Eye	Corneal Shape	Keratometry (steep meridian, flat meridian and difference)
A	"Normal", smooth variation in curvatures, low astigmatism.	47.87 D (7.05 mm) @ 77 ^{o} 47.60 D (7.09 mm) @ 167 ^{o} 0.27 D (-0.04 mm)
B	Regular astigmatism with the rule (moderate).	49.27 D (6.85 mm) @ 90 ^{o} 48.07 D (7.02 mm) @ 180 ^{o} 1.20 D (-0.17 mm)
C	Keratoconic, steep region of high curvature surrounded by lower curvatures.	54.50 D (6.19 mm) @ 65 ^{o} 54.10 D (6.24 mm) @ 155 ^{o} 0.40 D (-0.05 mm)
D	Regular astigmatism with the rule (severe).	47.69 D (7.08 mm) @ 88 ^{o} 44.36 D (7.61 mm) @ 178 ^{o} 3.33 D (-0.53 mm)

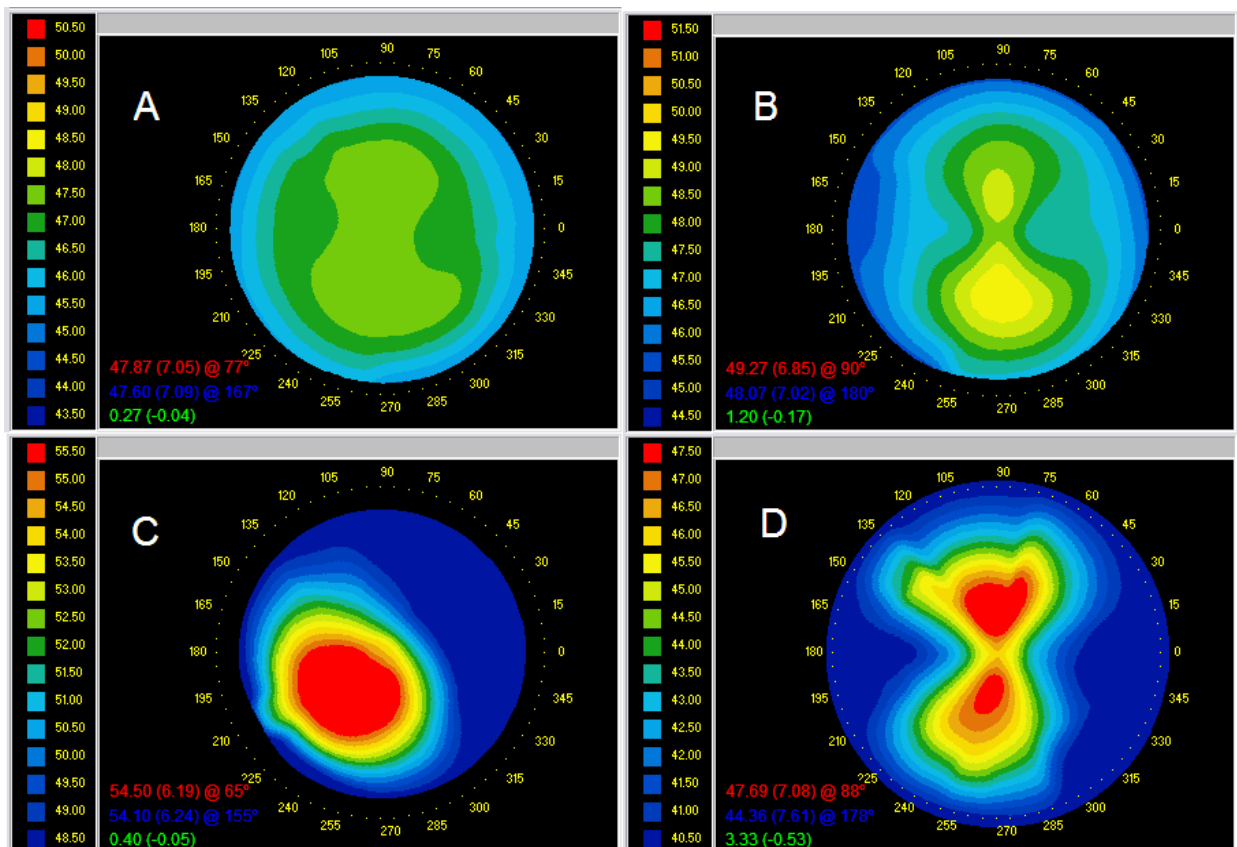Table 1. Keratometric data for the corneas used for ray-tracing.

Figure 4. Axial curvature maps for corneas shown in Table 1. The two-dimensional maps are color-coded in accordance to their respective carvature scales to the left (in diopters). The lower left values on each map are the same keratometry values shown in Table 1.

The four graphs in Figure 5 illustrate typical information which is useful for the analysis of the optical quality of the eye. These same graphs will be repeated for the other corneas (B, C and D) for comparison. The graphs are as following: (superior left - SL) Focal distances along optic axis Z versus pupil diameter; (superior right - SR) Radial size of retinal images (ρ_r) versus pupil diameter; (inferior left - IL) PSF for retinal image and (inferior right - IR) axial curvature

obtained directly from corneal topography files (*diop.txt* and *rho_c.txt*). We may notice from the SL graph that the focusing distance decreases as the pupil dilates, which is in accordance to the expected spherical aberration commonly present in the eye. The important fact in this graph is to notice the small difference in the curves for different semi-meridians, which also makes sense since this first cornea (A) has regular curvature and very low astigmatism. Nevertheless one may easily notice that curves for the vertical meridians (with the rule, angles 90^0 and 270^0) are closer to each other and slightly lower than curves for the horizontal meridian (against the rule, angle 0^0 and 180^0) which can be explained by the very low, but present, with the rule astigmatism of cornea (A) – see steeper meridian in map (A) of Figure 4. The SR is also in accordance to the expected variation in retinal image size for the four semi-meridians, i. e., a gradual increase in size as the pupil dilates and four curves very close to each other, as it should be for a "normal" cornea. The PSF in the IL graph follows quite closely (although in a negative sense) the pattern of corneal surface curvature, which is quite expected since corneal power is directly proportional to curvature (or inversely proportional to radius of curvature) – see equation (4). This is an important feature since it indicates that traditional curvature maps, which have been in use for quite a while by eye-care professionals, actually gives a good idea of the contribution of the cornea to image formation. Of course this is just an approximate view of what is happening in practice since we're not considering refraction by the lens and eye *in vivo* eye dimensions. The PSF shows symmetric and concentric rings, as expected and the IR graph shows a small variation in axial curvature from center to periphery of the cornea, with semi-meridians varying very closely.

In Figures 6-8 we print the same information as those for Figure 5 for the other eyes.

Notice in Figure 7 that focus and image size in SL and SR start close to each other for small pupils, become very distant apart for intermediate pupils (between 2-6 mm) and then, as the conic region on the cornea is very localized interiorly, these points rejoin on the periphery. Unfortunately during most periods of the day our pupils are in between 2-6 mm in diameter and become larger at night. For this specific eye a better visual quality may happen in very bright light situations during the day and at very low brightness such as when driving at night. Notice, again, that the PSF in IL follows very closely the pattern seen in the curvature map (Figure 4 (C)).

4 Discussion

Important information may be extracted from the graphs of Figures 5-8. We may observe a significant variation in the PSF plots for different corneas. In general terms there is a growing degradation of retinal image quality as the corneal surface becomes more irregular, which is clearly shown in the PSF images. Also, for the same corneal surface, the PSF has local variations in accordance to local smoothness or abruptness of corneal curvature and shape. Actually, this is probably a good explanation for the reasonably good refraction correction with sphero-cylindrical lenses even for cases of irregular astigmatism and keratoconus. This fact indicates that although the corneal surface might have high local variations in curvature and elevation, there are regions of reasonable smoothness that probably contribute for decreasing the distortion of the retinal image [22].

Comparing, for example, two cases that may be considered opposite in our examples, the "normal" and the "keratoconic" corneas, we may notice very distinct behavior. For the "normal" cornea the focal distance and retinal image size vary similarly for all semi-meridians. This means that the retinal image quality deteriorates uniformly for the entire corneal surface as the pupil dilates. Even if this patient is myopic or hyperopic, there is a greater chance of a better correction with any of the current methods available (PRK or LASIK, contact lenses or spectacles). The opposite happens to the keratoconic patient. It is easy to notice that once the pupil dilates there is a totally different behavior for different semi-meridians. For small pupils the focal distances are very close but as the pupil dilates, for certain meridians the focal point is brought closer to the cornea, but for others they are positioned further away. And for the keratoconic case this is even worse, as we may notice, compared to astigmatism, given that keratoconic corneas behave as coma like surfaces, that is, they have no axis of symmetry, making it hard for the accommodation system to find a region of *least confusion*.
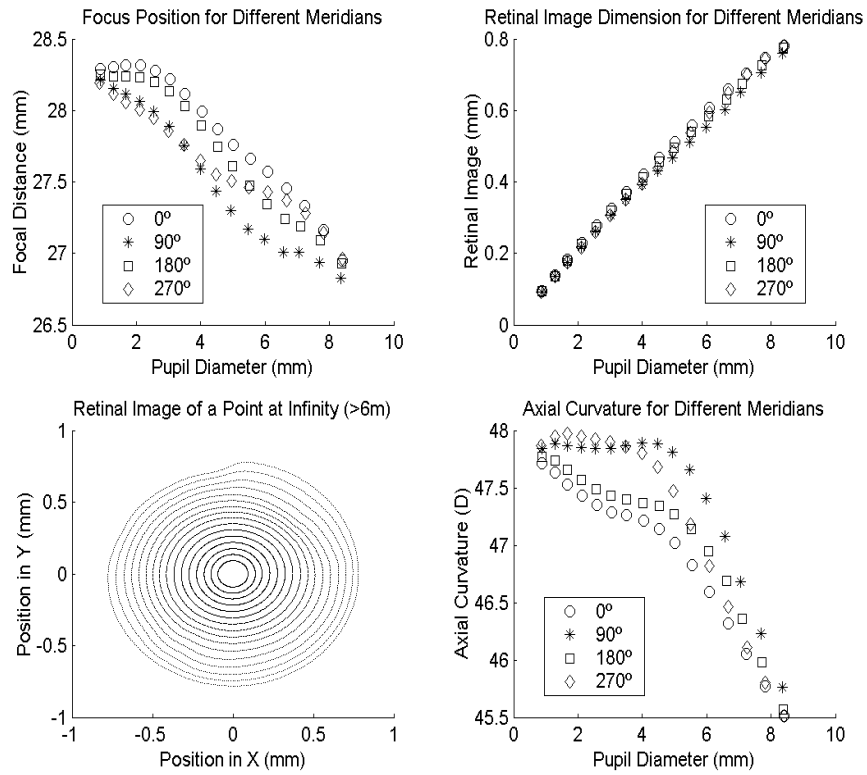
Figure 5. Results of ray-tracing for first eye (A).
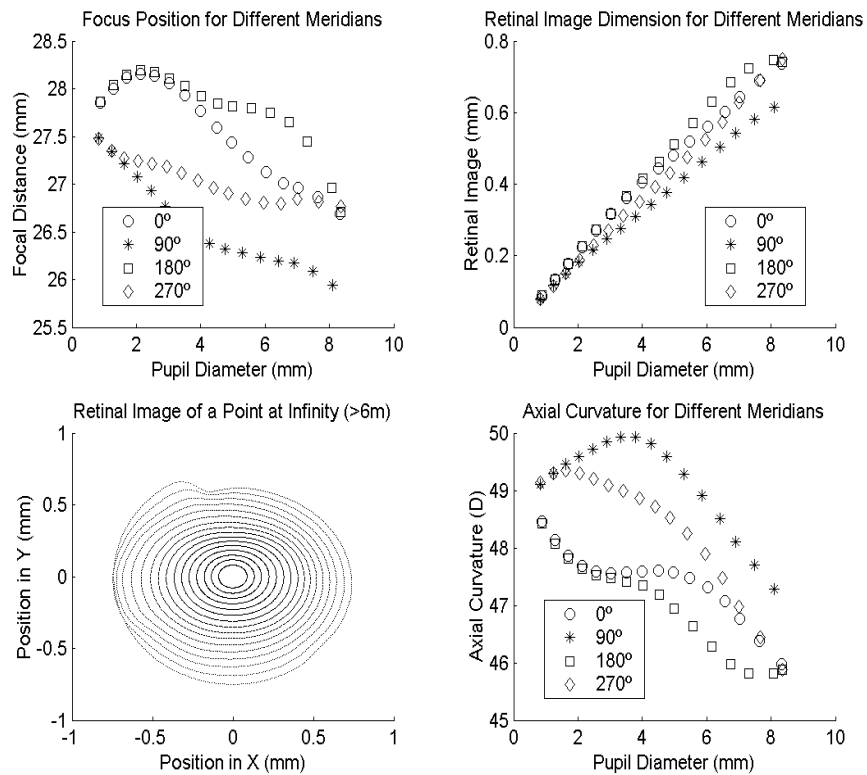

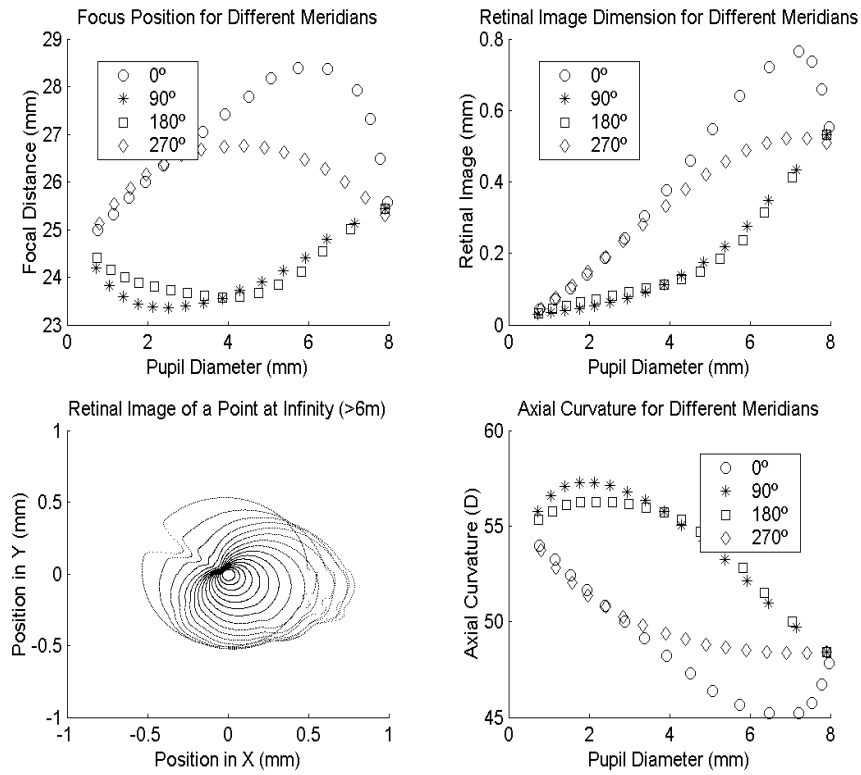Figure 6. Results of ray-tracing for second eye (B).

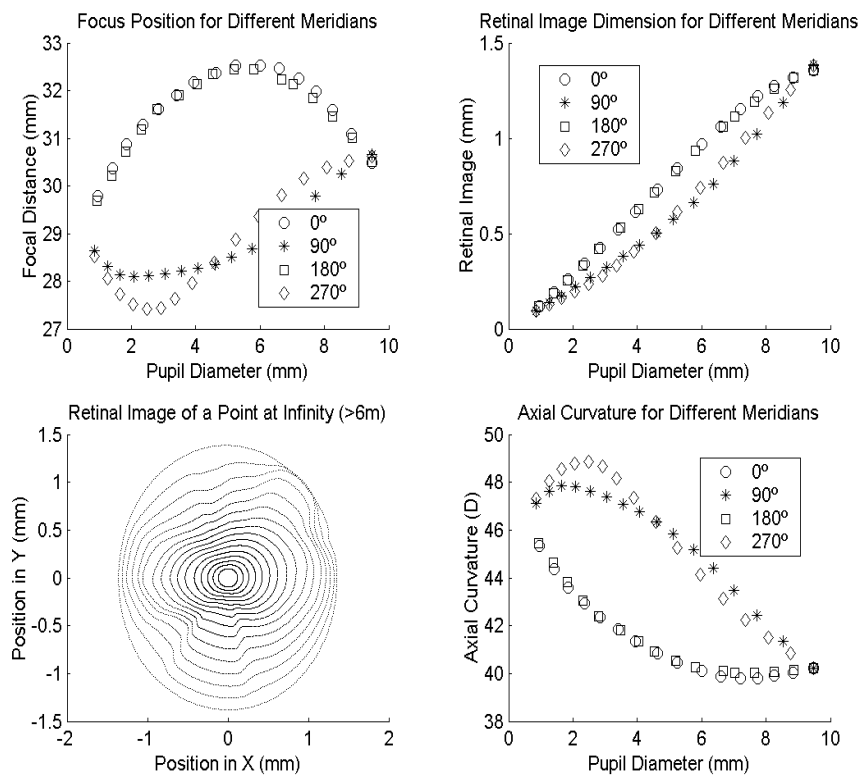Figure 7. Results for Keratoconic cornea (C).

Figure 8. Results for the severe astigmatic cornea (D).

It is important to notice that the simulations implemented in this work are not actual measurements of the retinal image quality of *in vivo* patients, but otherwise a close study of the aberrations caused by corneal irregularities that are present in common eyes found in healthy populations. This is so because we used *in vivo* corneal topography data in a schematic eye that has dimensions based on mean statistical data of the population. Another important fact is that we do not consider here the lens and therefore accommodation factors, and also differences in refractive indexes of the interior components of the eye. An equivalent refractive index is used for the entire eye in the accommodated state, which we know is not the case for the human *in vivo* eye. Nevertheless this model is a reasonable approximation to the human accommodated eye since 2/3 of our refraction occurs at the air-corneal interface.

More accurate eye models [19] and even Physical optics (using waves) [22] should be considered, taking into account not only the shape of the anterior and posterior lens surface and thickness, but also the variation of these parameters with accommodation [23] and with age [24, 25]. Also, by collecting results from a wave-front device and the corneal topographer one may input data in the algorithms presented here in order to estimate the Zernike coefficients of the optical aberration contribution of the crystalline lens.

Acknowledgements

References

[1] Scheiner C, Sive fundamentum opticum, Innspruk, 1619.

[2] Helmholtz von HH (1909) Handbuch der Physiologishen Optik. In Southall, J.P.C. (Translator), Helmholtz's treatise on physiological optics (1962). New York: Dover.

[3] Stone, J., The Validity of Some Existing Methods of Measuring Corneal Contour
Compared with Suggested New Methods, *Brit. J. Physiol. Opt.*, 1962;19:205-230.

[4] Le Grand, Y., El Hage, S. G., *Physiological Optics*, Springer Series in Optical Sciences, Springer-Verlag, 1980;13.

[5] Placido, A., Novo Instrumento de Exploração da Cornea, *Periodico d'Oftalmológica Practica*, Lisboa, 1880;5:27-30.

[6] Gonzales RC, Woods R. E., Digital Image Processing, Addison-Wesley,1992.

[7] Carvalho LA, Stefani M, Romão AC, Tonissi S, Castro J, Digital Processing of image reflectd from the Lachrymal Film of the Anterior Corneal Surface, Revista Brasileira de Engenharia Biomédica, v.17, n. 3, 113-123, set/dez 2001.

[8] Klyce S.D., Computer-Assisted Corneal Topography, High Resolution Graphics Presentation and Analyses of Keratoscopy, *Invest. Ofthalmol.Vis. Sci.*,1984;25:426-435.

[9] Mandell, R. B., York, M. A., A New Calibration System for Photokeratoscopy, *Am. J. Optom.*, 1969, 46(11):818-825.

[10] Krueger PR, In perspective: Eye tracking and Autonomous laser radar, J. Refract Surg 1999;2:145-149.

[11] Pettit G. H., Campin J.A., Housand B. J., Liedel K. K. - Customized corneal ablation: wavefront guided laser vision correction, AUTONOMOUS TECHNOLOGY (ORLANDO, FL) ARVO (The Association for Research in Vision and Ophthalmology), Annual Meeting, Fort Lauderdale, Florida (USA), May 9-14,1999.

[12] Thibos LN, The prospects of perfect vision, Journal of Refractive Surgery, Vol. 16, September/October 2000, 540-545.

[13] Maria Cristina Ferreira de Oliveira, Rosane Minghim, Uma Introdução à Visualização Computacional, XVI JAI - Jornada de Atualização em Informática, Brasília-DF, 2-8 Agosto de 1997, p. 85-127.

[14] Rogério Eduardo da Silva, "Um Simulador para o Sistema Visual Humano usando Ray Tracing", master degree Thesis presented at the ICMC- USP, Brazil, March, 2001.

[15] Carvalho LAV, Tonissi SA, Romão AC, Santos LE, Yasuoka F, Oliveira AC, Schor P, Chamon W, Castro JC, Desenvolvimento de um Instrumento Computadorizado para Medida do Poder Refrativo da Córnea (Videoceratógrafo), Arq. Bras. Oftal., Dezembro/1998;61(6).

[16] L. A. V. de Carvalho, S. J. de Faria e Souza e Jarbas C. Castro, Desenvolvimento de um sistema para medida da curvatura da córnea durante o ato cirúrgico, RFAI, 1996,11:119-126.

[17] William J. Schroeder, Kenneth M. Martin, Lisa S. Avila, C Charles Law, The Visualization Toolkit User's Guide, Version 4.0 (with CD-ROM)
by, Kitware, Inc., December 2001.

[18] The Visualization ToolKit (VTK) is an open source, freely available software system for 3D computer graphics, image processing, and visualization. VTK includes a textbook published by Prentice-Hall (The Visualization Toolkit, An Object-Oriented Approach To 3D Graphics, 2nd edition" ISBN 0-13-954694-4). More information may be found at: http://public.kitware.com/VTK/what-is-vtk.php

[19] Doshi JB, Sarver EJ, Applegate RA, Schematic eye models for simulation of patient visual performance, J Refract Surg 2001 Jul-Aug;17(4):414-9, Erratum in: J Refract Surg 2001 Sep-Oct;17(5):498-9.

[20] Carvalho, L; Tonissi, SA; Castro, JC; Preliminary tests and construction of a computerized quantitative surgical keratometer, J Cataract Refract Surg 1999; 25: 821-826.

[21] Roberts C, The accuracy of 'power' maps to display curvature data in corneal topography systems, Invest Ophthalmol Vis Sci 1994 Aug;35(9):3525-32.

[22] Garcia DD, Van de Pol C, Barsky BA, Klein SA, Wavefront Coherence Area for Predicting Visual Acuity of Post-PRK and Post-PARK Refractive Surgery Patients, SPIE conference on Ophthalmic Technologies IX, San Jose, California, January 1999; Proc. SPIE Vol. 3246, p. 290-298, Ophthalmic Technologies VIII, Pascal O. Rol; Karen M. Joos; Fabrice Manns; Eds. ; Publication date: 6/1998.

[23] Brown N (1973) The change in shape and internal form of the lens of the eye on accommodation, Exp. Eye Res., 15, 441-459.

[24] Koretz JF, Handleman GH (1986) Modeling age-related accommodative loss on the human eye. Mathematical Modelling, 7, 1003-1014.

[25] Koretz, J.F. and Handelman, G.H. 1988. How the human eye focuses. Scientific American 256 (7): 92-99.